is being made. In addition to the use of the nanoparticles in gas sensing, numerous advancements were made in the field of science and engineering using these nanoporous materials.

The porous nature of the oxide films were first exploited in 1950's after the invention of the electron microscope. Keller et.al (1953) described that the porous structures contained uniformly spaced hexagonal structures.

Some of the nanoporous sensors used in various fields of sensing include detection of cancer cells, humidity and ammonia gas sensing application, etc. (Kiran Bhattacharyya, 2012) mentioned a method to detect initial cancer cell in the human body. Gold nanoparticles have an interesting property that makes them ideal in detection of cancer cells. This property is to scatter the absorbed light. Many cancer cells exhibit a receptor (EGFR) all over their surface. These receptors can be used as targets in detection of cancer cells. By binding the gold nanoparticles to the antibody of EGFR, the nanoparticles target and patch to the cancer cells. Once it is attached to the cancer cell the gold nanoparticle will reflect light when exposure to light, differentiating between healthy cells and the cancer cells. These gold nanoparticles are not only used for the detection of cancer cells but also used for many different purposes, like curing of diseases, detection of proteins, vapor detection, etc. The nanoparticles are not only used in detection of the cancer cells but can also act as drug delivery systems by detecting the cancer cells and directly delivering the medicine to the targeted site.

The porous nature of the oxide films were first exploited in the 1950s after the invention of the electron microscope. Keller et.al(1953) described that the porous structures contained uniformly spaced hexagonal structures. Later work on controlling the pore diameter and interpore spacing on the anodization voltage was done. Later refinements on fabricating ordered porous alumina with defined pore structure was done using different electrolytes, namely malonic acid,

and was demonstrated that use of malonic acid resulted in corrosion resistant characteristics (Lee, 2007). These AAOs are used in numerous applications, mainly for humidity sensing.

Oomman K.Varghese(2002) demonstrated humidity and ammonia sensing using nanoporous alumina films. It also demonstrated the effect of pore size and uniformity on the response of the nanoporous alumina in ammonia and humidity sensing. It was demonstrated that the sensor with smaller pore diameter is sensitive to wide range of humidity values and also showed more sensitivity for ammonia (Oomman K. Varghese, 2002). The study also included the mechanism of conduction through the porous alumina. It said that the alumina senses the presence of the ammonia based upon ionic conduction. Ionic conduction is a mechanism of movement of ions of the analyte from one site to another through the vacancies. This ionic conduction at the surface of the alumina decreases the overall sensor impedance by donating electrons to the conduction band in the base material.

1.4 ANODIZED ALUMINA OXIDE (AAO)

While using ceramics with various metal oxides including alumina, mainly for humidity sensing, experimentation was done with anodized aluminum oxide (AAO) (Martin Kocanda et.al, 2009) in sensing various analytes. It was demonstrated that the AAO showed response to these analytes where the analytes were alcohols and cyclic volatile compounds. Anodized alumina oxides consist of two layers; the below layer is a metal oxide layer and the above layer is a porous layer grown from the oxide layer.

Nanoporous anodized aluminum oxide has gained much importance due to its physical and chemical properties. The pore structure can be controlled by using different electrolytic solutions

devices and many electronics. This may be because silica is most abundant material on the earth and is cost effective. Porous silica gained much importance due to its quantum effects identified by Ulrich Gösele and V. Lehmann(1991). These porous silicon structures are fabricated by the process of electrochemical etching (Losic, 2015). Mixtures of hydrogen fluoride (HF) and nitric acid (HNO_3) have been widely used. Initially it is required to remove any formation of the oxide layer on the commercially available silicon wafer is important as it may act as contaminants during etching. Immersing the wafer in HF solution may remove all the impurities and make the wafer perfect for the etching. So as the wafer is free from impurities an etching cell must be set up for the etching process. In this process metals like gold and platinum are to be selected as the etching element as they are inert. At this step etching is done by placing the silicon wafer in the test cell and exposing it to HF solution with the platinum immersed inside the HF solution. Thus the fluoride (F^-) ions form bonds with the silicon (Si) thus creating an electron hole on the substrate leading to the formation of porous silicon. The porous silica was used for applications as biosensors, for drug delivery, in optical sensors, etc. Many advancements were made in the fabrication process of the porous silicon and anodized alumina oxides (AAO) in regulating the pore size and thickness of the film. In AAO the anodization potential and the electrolyte amount variation may lead to the formation of well-defined pores. It was demonstrated by Varghese et.al (Oomman K. Varghese, 2002) single-step anodization resulted in more disordered pores whereas double-step anodization process resulted in ordered and smaller pores.

1.5 Nanoporous Organosilicate (NPO) Films

Further on there are many types of synthesis processes like colloidal method, sol-gel, porogen approach and surfactant templating. These methods prove to be competitive due to their

low cost of the precursors, complexity of kinetics, repeatability, and time required for the fabrication (Chitra Agashe, 2008). As any application requires a fast-obtained yield at low cost with no compromise on the sensor characteristics, nanoparticle-polymer composites were considered. These nanoparticle-polymer composites have advantages in optical, electrical and mechanical properties (Anna C. Balazs, 2006). It was demonstrated that the nanoparticles could be self-assembled due to the collision nature of the ligands on the nanoparticle surfaces. Nanoporous organosilicate (NPO) films are based upon this concept of nanoparticle-polymer composites. As fast-integrating circuits are necessary for the faster sensing, low dielectric (*k)* constant films are to be used instead of the metal oxide devices. Among many materials that are tried in replacing these metal oxides, PMSSQ is one of the most widely researched materials because of its compatibility in fabrication of the film, thermal stability and its hydrophobic nature. It was stated that PMSSQ has a dielectric constant of 2.6-2.8 which could be further reduced upon decreasing its density (Hyeon-Lee, 2005). The density of the PMSSQ can be varied by introducing pores into the PMSSQ nanoparticles, thus reducing the overall nanoporous film. But as the mechanical strength is important for any film to integrate into the electronic devices as a sensing device, these PMSSQ are mixed with a precursor solution. This precursor solution is mainly a polymer that could increase the durability and mechanical strength to the film. One of the main advantages of the PMSSQ-based films is the hydrophobicity. The metal oxides have a tendency to adsorb moisture from the atmosphere and thus degrade in their performance, whereas the PMSSQ based films being naturally hydrophobic doesn't have the capability to adsorb moisture, thus increasing the efficiency.

1.6 Preparation of NPO

The material extensively used for the nanoporous organosilicate films deposition contains the polymethyl silsesquioxane (PMSSQ), polypropylene glycol (PPG), propylene glycol methyl ether acetate (PGMEA). As PMSSQ is hydrophobic, these PMSSQ molecules are bound together by PPG forming a network-like structure during the porous film formation. The basic methodology of pore formation here is the porogen approach where a pore generator (porogen) is chosen such that evaporation of this porogen results in the formation of porous NPO.

The nanoporous film was prepared using a heat decomposition method to produce films from suspensions of polymethyl silsesquioxane (PMSSQ; Techneglas) nanoparticles in polypropylene glycol (PPG; m.w. 425), which was dissolved in propylene glycol methyl ether acetate (PGMEA) (Korampally, 2009). This method allows for the control of the film porosity and film thickness by controlling the by-weight concentrations of PMSSQ and PPG in the precursor solutions and by controlling the temperature used for decomposition.

NPO films used for the work discussed in this chapter were a 5555 solution, which had a 5:5 weight ratio of solvent (PMA) to solute (PPG and PMSSQ), where the solute had a 5:5 weight ratio of PPG to PMSSQ. All films were spin coated onto the silicon wafer substrates at 3000rpm/30sec and then decomposed by placing the coated wafers on a hotplate at 500°C/5min (Figure 4). During this decomposition process, due to the heat the PMSSQ nanoparticles attain Brownian motion and are self-assembled crosslinking with other PMSSQ molecules to form porous film. Wafers were then air cooled to room temperature.

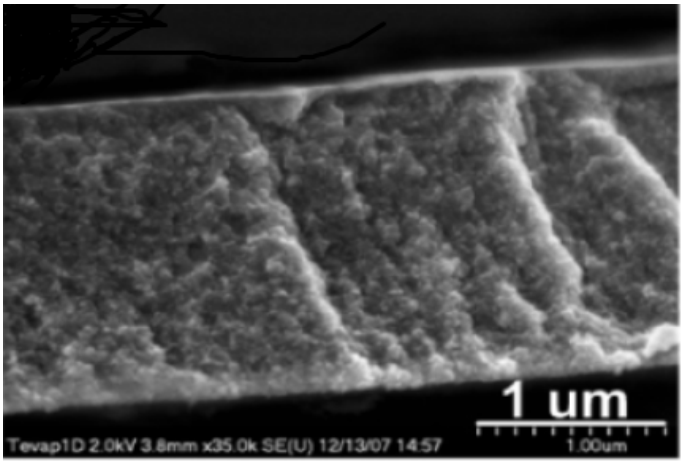

Figure 5 SEM image of the cross sectional view of NPO 1 μm magnification

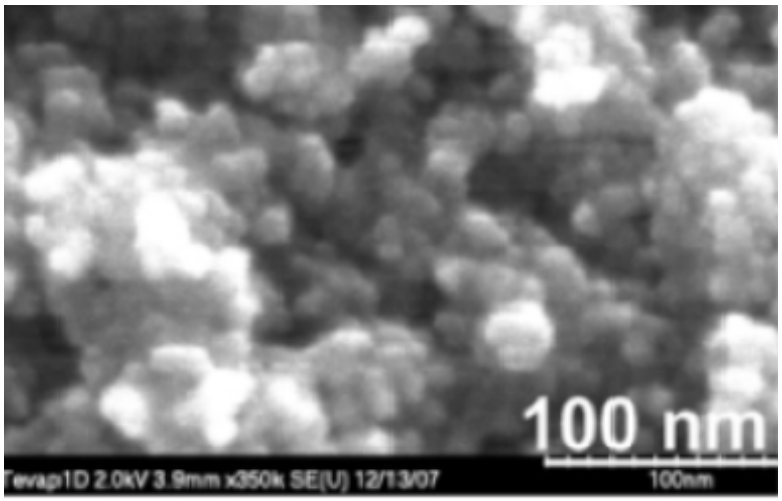

Figure 6 SEM image of the cross sectional view of NPO 100 nm magnification

The conduction mechanism in the nanoporous organosilicate sensor within the subtract size of about 10nm was extensively gaining prominence related to offering two distinct benefits over

the planner material that is related to integrating the scheme of sensing that has the following characteristics:

1. Broad surface area
2. Capillary condensation

Capillary condensation is a process of condensation of vapour at the porous membrane. The vapor condenses at the surface of the porous film (liquid-vapor interface) due to the Van der Waal's forces acting between the substrate and the vapor. After this condensation, the liquid adsorbed onto the surface of the NPO increases the overall sensor conductance increase, leading to the change in the sensor response.

1.7 Impedimetric Sensing

The sensor response is always measured in terms of real and imaginary impedances, namely Nyquist plot. These plots are plotted with real impedance on x-axis and imaginary impedance on y-axis. Thus to measure a response of a sensor, measuring impedance is necessary. This measurement of impedance for analyzing a sensor response is called impedimetric sensing and measured using impedance spectroscopy.

1.7.1 Impedance Spectroscopy

The impedance spectroscopy contains the source of the variable programmable frequency that provides the ability for the generation of a sinusoidal alternating current waveform with the adequate amplitude level to efficiently excite the sensors (GamryInstruments).

Over the past two decades, electrochemical impedance spectroscopy (EIS) has emerged as the most powerful of electrochemical techniques for defining reaction mechanisms; however, most of the work was done in analyzing the system response in liquid-electrode interface. The impedance spectroscopy came into theory in 1894 with the application of Wheatstone bridge by Nernst for calibration of dielectric constant for different electrolytes (The Electric World, 1987). This approach was later implemented to calculate dielectric constants of the galvanic cells, diffusion mechanism, etc. In 1920 it was implemented on biological systems and it was observed that there is relation between the frequency component of impedance and constant phase angle. Later on two brothers, Cole and Cole, suggested that this relation is in the form of a depressed semicircle (Licker, 2005). From then the impedance spectroscopy was used in the field of electrolytes, chemical solutions, rotating disks and many other fields for the analysis of the system response based on the Cole-Cole plot. The impedance spectroscopy has wide range of applications which cannot be mentioned in detail.

1.7.2 Working Principle of Impedance Spectroscopy

The basic working of the impedance spectroscopy relies on a Wheatstone bridge (MarkE.Orazem, 2011). This bridge is used to measure the impedance of the measurand by adjusting resistor and capacitor at each frequency. A signal generator generates a sinusoidal signal based upon the input parameters and is applied to the sensor, thus obtaining the sensor response in terms of real impedance and imaginary impedance. In earlier stages different components are used for these operations but as of now all of them are embedded into a single system. The obtained

sensor response is represented as Nyquist plots or Cole-Cole plots with the real impedance on x-axis and imaginary impedance on y-axis respectively.

Figure 7 shows a typical representation of the Nyquist plot of a parallel RC network. However, practically a perfect semicircle is not obtained. It represents the real impedance on x-axis and imaginary impedance on y-axis. ω is the frequency with lowest frequency on the right and highest frequency on the left.

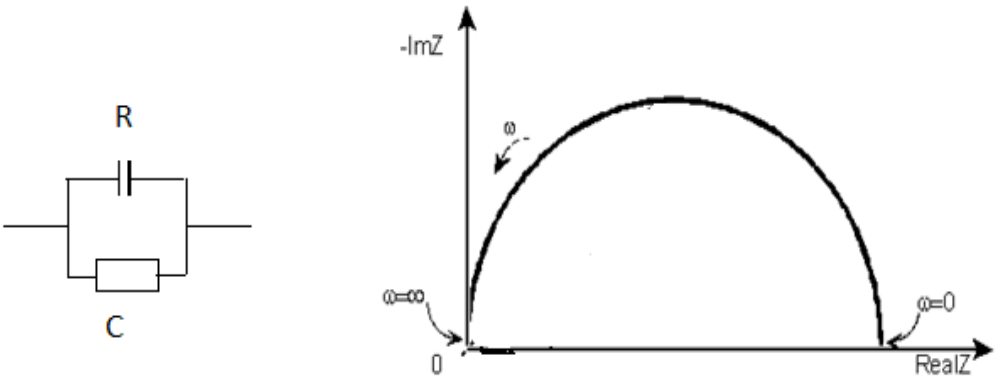

Figure 7 Typical representation of a Nyquist plot of a parallel RC network

Electrochemical impedance spectroscopy is a useful tool when a number of analyses are to be done using a single response.

1.7.3 Advantages and Disadvantages of EIS:

Advantages of EIS include:

- Time optimization
- Less apparatus

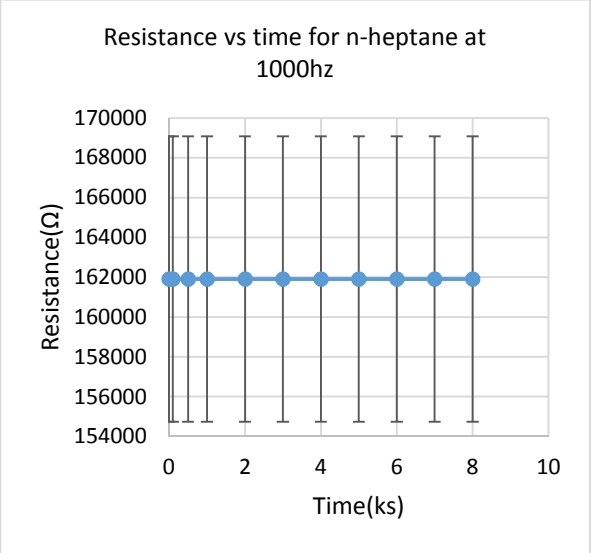

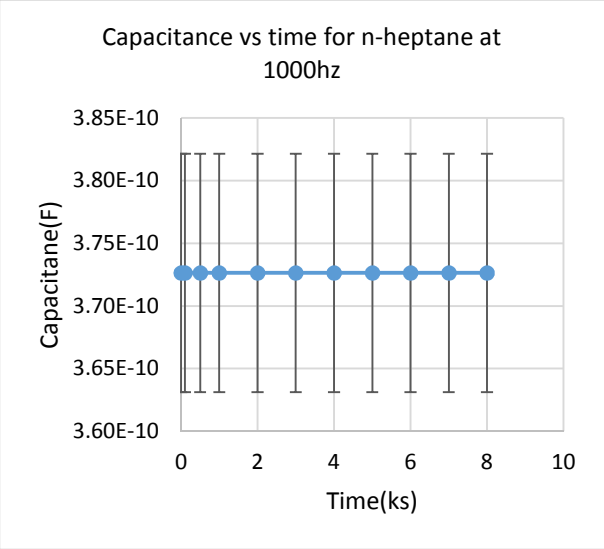

Figure 15a, 16b Represents typical response of NPO sensor in n-heptane with resistance and capacitance measured in time domain

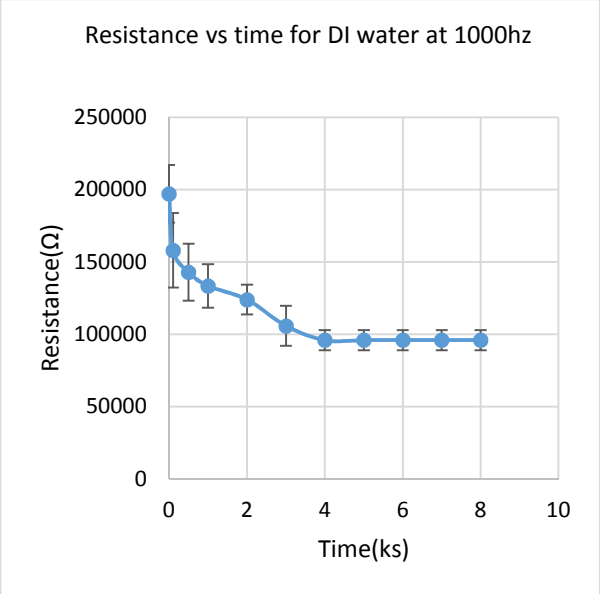

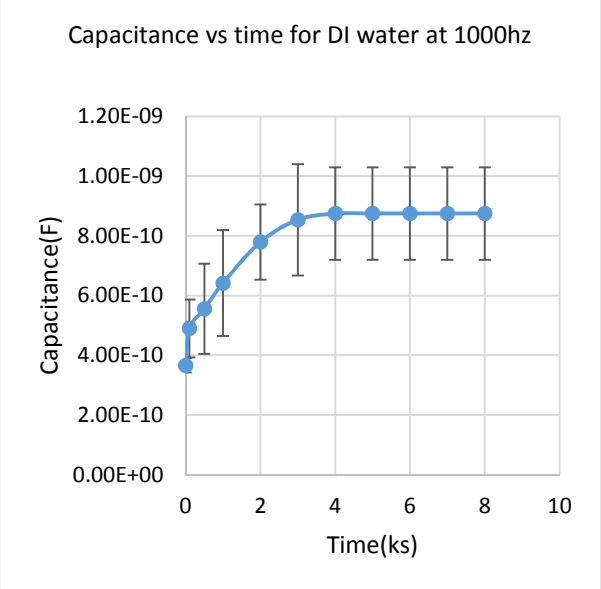

Figure 16a, 17b Represents typical response of NPO sensor in n-heptane with resistance and capacitance measured in time domain

The measured real impedance and imaginary impedance values are plotted separately with respect to time on x-axis (abscissa) and real or imaginary impedance on y-axis (ordinate). Similar data trend was observed for frequencies 500 Hz and 10 KHz with shift in their initial resistance and capacitance values. Examination of the data indicated that sensor response in methanol achieved stability at ≈630s, faster than in any of the solvents. This may be because methanol is more polar and lighter than isopropanol. Response in methanol (at ≈632s) and isopropanol (at ≈3000s) stabilized faster than the DI water because of the fact that both methanol and propanol are less polar than water due to the presence of non-polar carbon-carbon bond. Though the NPO sensor at this stage is hydrophobic, it showed response to DI water, as water contains H^+ ions and OH^-; H^+ ions are mainly responsible for wetting which may form bonds with the NPO surface by Van der Waal's force. It is also known that the adsorption mechanism in NPO films is mainly due to capillary condensation, where even the polar compounds can be adsorbed leading to the response with DI water as depicted in Figure 16. Important aspect to be noted in Figure 17 is the sensor showed no response when exposed to n-heptane. Initially it was assumed to be very low response that cannot be noticed, but it was proved to be wrong in the latter when the sensor is subjected to frequency sweep from 500 Hz to 10 KHz at 100mV(p-p) sinusoid.

The sensor is subjected to each vapor for three different trials to ensure recurrence. Error bars are plotted taking into consideration these three trials. Standard deviation (SD) at every measured time interval is calculated and error bars are accordingly plotted.

$$\sigma = \sqrt{\frac{\sum_i^N (x_i - \mu)^2}{N}}$$

Where σ = Standard deviation, μ = mean of all the values, x= individual value in the data set, N = total number of values in the data set

Figures 18 represents the measured resistance for frequencies of 500 Hz, 1 KHz and 10 KHz at 100 mV (p-p) sinusoid. It could be demonstrated that the real impedance (resistance) value decreases continuing onto higher frequencies comparatively with high impedance values at lower frequencies. This could be used to indicate the operating range of the NPO sensor, making it more operational at lower frequencies. In Figure 18 as the frequency approached 10 KHz, the resistance value is ≈0.

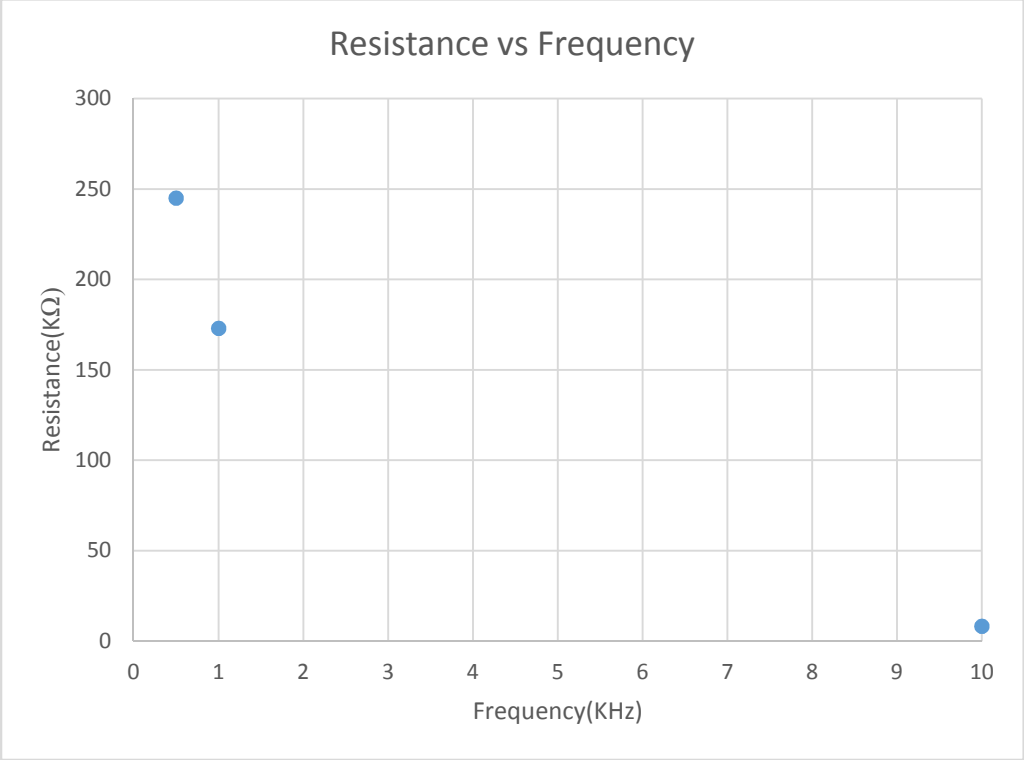

Figure 17 Comparison of the real impedance value of NPO at various frequencies

For the analysis of the adsorption of the analytes onto NPO substrates, a subsequent Nyquist plot or Cole-Cole plot is obtained by a frequency sweep of 100 Hz to 10 KHz with 31 intermediate points at which the real and imaginary impedance values are electronically recorded. The frequency sweep is performed upon stabilization of the NPO in each analyte. Figure 19 represents a Nyquist plot of the hydrophobic NPO sensor with respect to vapor - phase analytes. It is noticeable that the response in n-heptane coincides with the response of NPO in air (baseline), indicating that the NPO irresponsive to n-heptane may be due to very high vapor pressure, thus remaining in vapor - phase even after getting adsorbed onto the NPO, and also may be because of the lacking free H^+ ions which are mainly responsible for wetting. The hypothesis of not much distinction is observed among the analytes considered for the experiment because the NPO film is

hydrophobic. Further work was required to analyze the impedance spectroscopy responses of the same analytes if the NPO was hydrophilic. For this purpose, as an advancement to the initially fabricated NPO sensor, the NPO is exposed to mild CO_2 plasma (as mentioned in Section 2.5) for 45sec at 429 mTorr. Now that the NPO substrate is plasma treated, the surface of the NPO is hydrophilic.

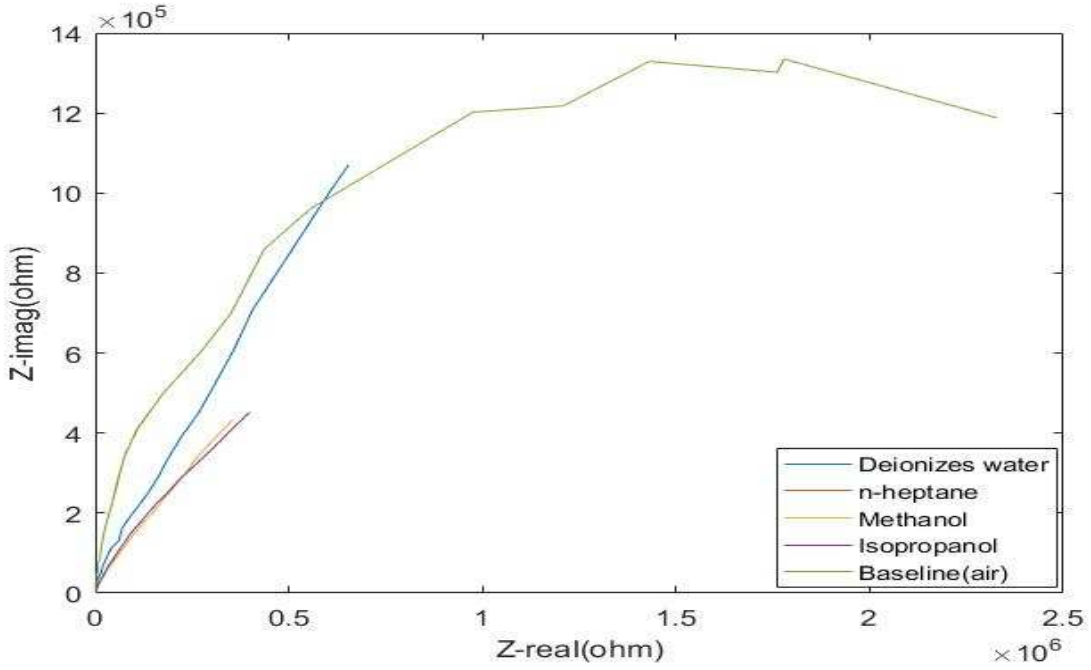

Figure 18 Nyquist plot showing frequency response of hydrophobic NPO sensor in methanol, isopropanol, n-heptane, DI water and air (baseline)

3.3 Response of the Hydrophilic NPO

The same set of experiments as is done with the hydrophobic NPO is done with the plasma-treated NPO (hydrophilic) and compared. It was observed that the analytes showed better response with the plasma - treated NPO. The plasma - treated NPO is placed in the test cell (glass vial) and connected to the external sensing setup. For each of the analyte taken, resistance and capacitance

values are electronically recorded and used for further analysis. All of the experiment is done at a setting of 100 mV (p-p) sinusoid for a time period of 8000 sec (until the response is unconditionally stabilized). Again considering three frequencies (500 Hz, 1 KHz and 10 KHz), graphs were obtained for the tabulated resistance and capacitance of the plasma - treated NPO sensor.

The Figure 20 represents the resistance value of the NPO sensor (plasma - treated) with frequencies of 500 Hz, 1 KHz and 10 KHz. When compared with Figure 18 the resistance at all the frequencies is more than double, thus supporting better sensing characteristics of the hydrophilic NPO sensor (because higher resistance implies higher resistivity to the flow of charge).

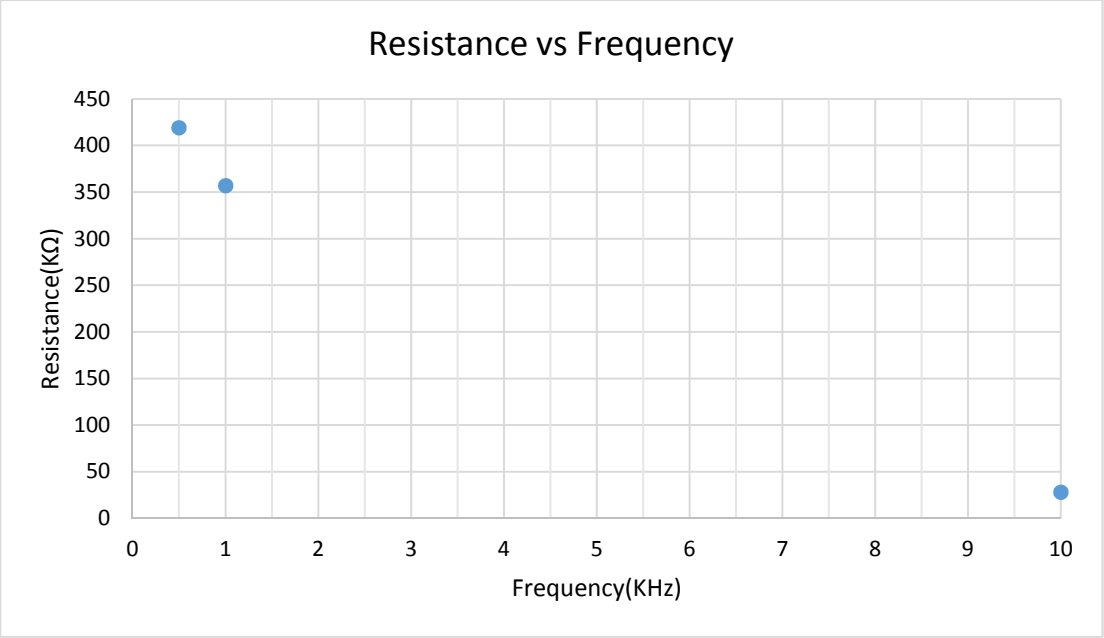

Figure 19 Representation of the plasma - treated NPO response in air at frequencies of 500 Hz, 1 KHz and 10 KHz in terms of resistance

Figures 21 to 24 represent the response of the NPO sensor after plasma treatment in different analytes. It is evident that the sensor is responsive to every analyte irrespective of the level of sensitivity. This supports that the hydrophilic NPO sensor can be used in sensing various analytes. These responses show comparatively smaller error bars than that of the hydrophobic NPO sensor responses in Section 3.2, supporting more recurrence at this stage. Error bars are obtained as mentioned in the Section 3.2 by taking the standard deviation (SD) and the response plotted with the mean of all the three trials. A Nyquist plot or Cole-Cole plot is obtained by subjecting the NPO sensor to various analytes. It is made sure that the response is electronically recorded after the sensor is stabilized.

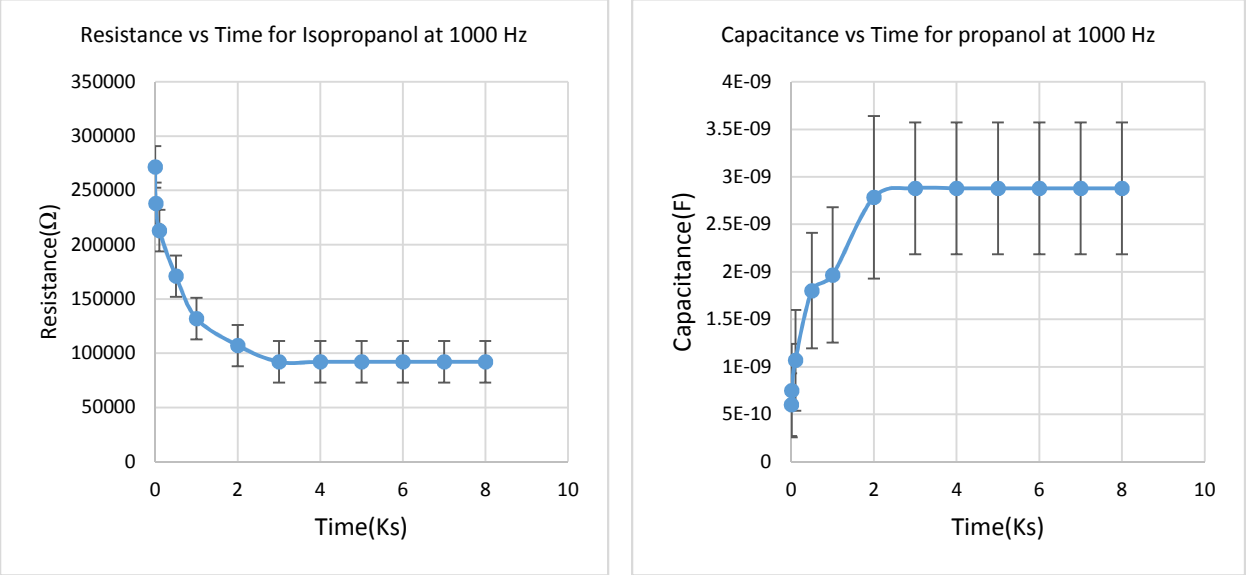

Figure 20a,b Represents typical response of hydrophilic NPO sensor in isopropanol with resistance and capacitance measured in time domain

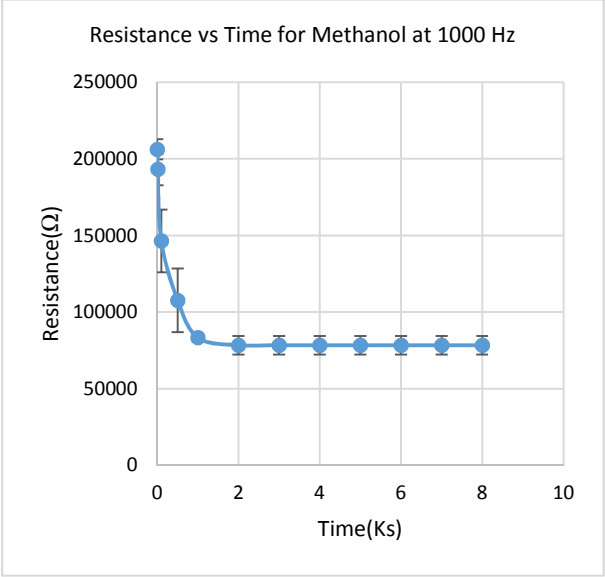

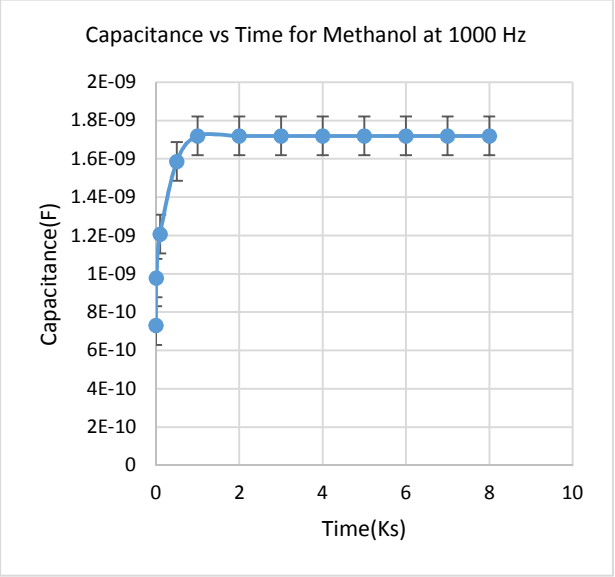

Figure 21 a, b Represents typical response of hydrophilic NPO sensor in methanol with resistance and capacitance measured in time domain

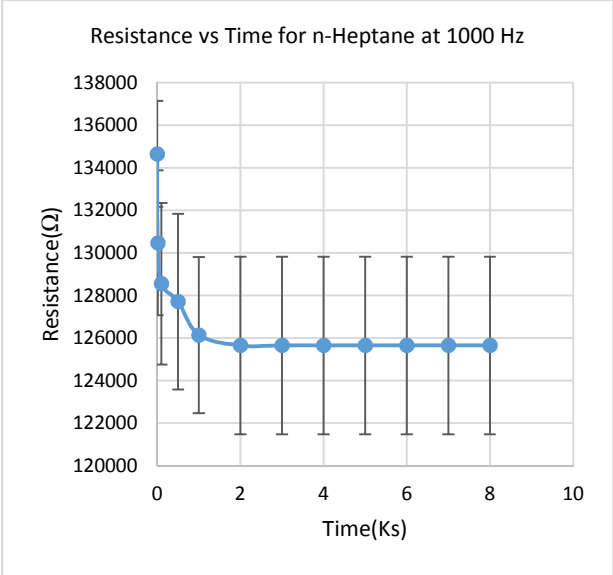

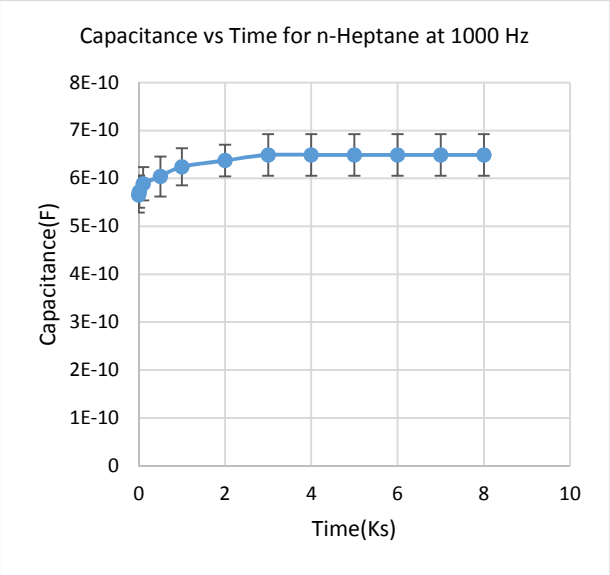

Figure 22 a,b Represents typical response of hydrophilic NPO sensor in n-heptane with resistance and capacitance measured in time domain

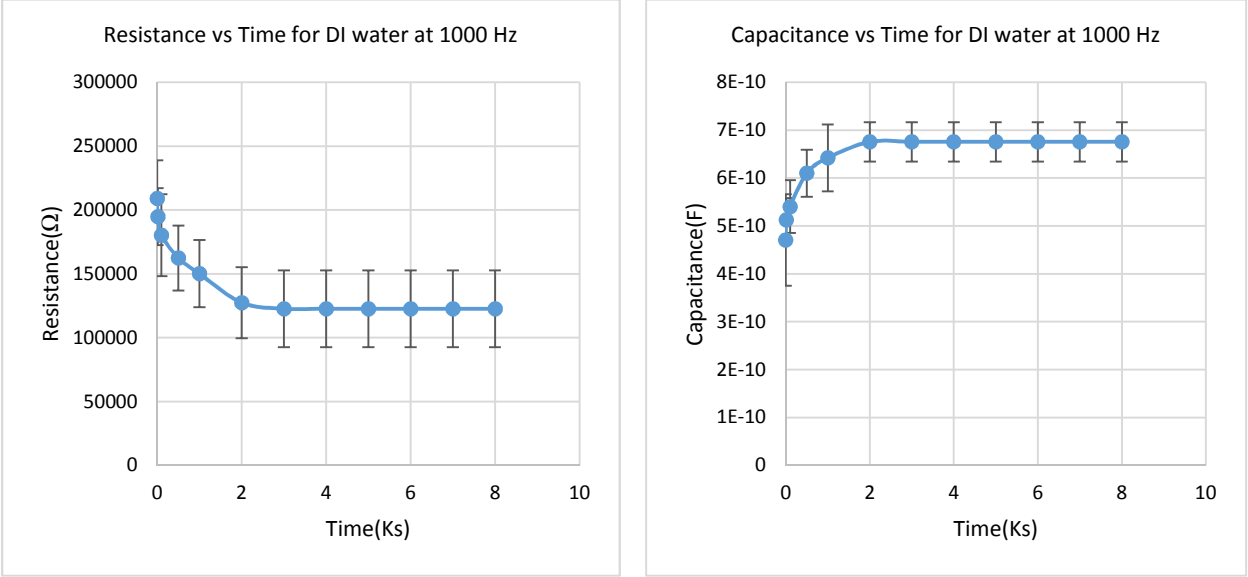

Figure 23 a,b Represents typical response of hydrophilic NPO sensor in DI water with resistance and capacitance measured in time domain

Figure 25 represents the Nyquist plot recorded at a frequency sweep from 100 Hz to 10 KHz with 100 mV (p-p) sinusoid. This plot gives us a conclusion that the sensor response is in the form of a typical parallel RC circuit with a purely resistive response after 10 KHz.

The analytes were clearly distinguished by the NPO with dominating separation from the baseline. There is a preferable gap between the baseline and the response in the analytes, namely DI water, methanol and isopropanol. A predictable response is where the alcohols and DI water have lower real and imaginary impedance compared to the organic aliphatic compounds. However n-heptane didn't show appreciable response even for the hydrophilic NPO.

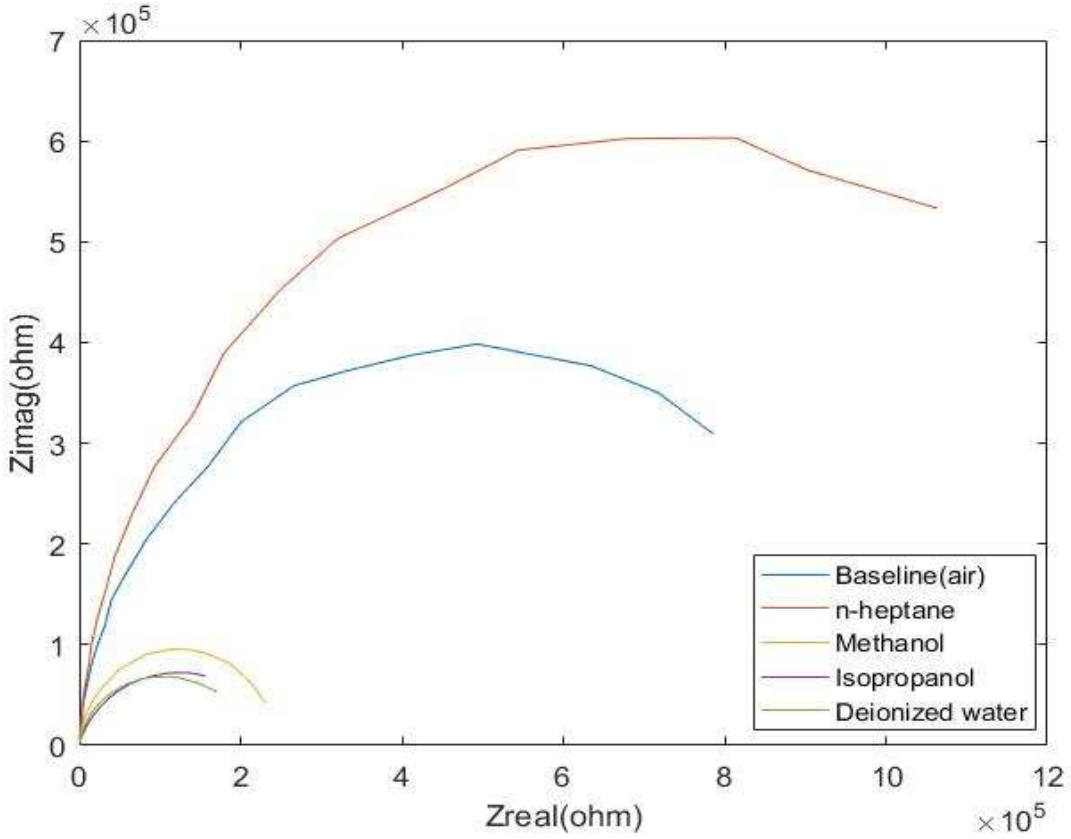

Figure 24 Nyquist plot showing frequency response of hydrophilic NPO sensor in methanol, isopropanol, n-heptane, DI water and air (baseline)

Table 1 shows the polarity index of the analytes, with water having the highest polarity and n-heptane having least polarity. Polarity index represents the ability of the compound to reach with various polar compounds. Low polarity index of n-heptane may be the cause for less response of the n-heptane onto the NPO. However Figure 26 shows the relation between the response and the polarity index: response shifts away from the baseline in analyte with higher polarity index. The graph also shows the trend with the relative permittivity, as mentioned for the AAO in the literature, with highest permittivity analytes having more shift. Figure 26 represents the Cole-Cole plot obtained for an AAO sensor on exposure to various chemical analytes.Table 2 represents the relative permittivity of the analytes.

Table 1 Value of the Polarity Index of the analytes

Name of the analyte	Polarity Index
Water	10
Methanol	5.1
Isopropanol	3.9
n-heptane	0.1

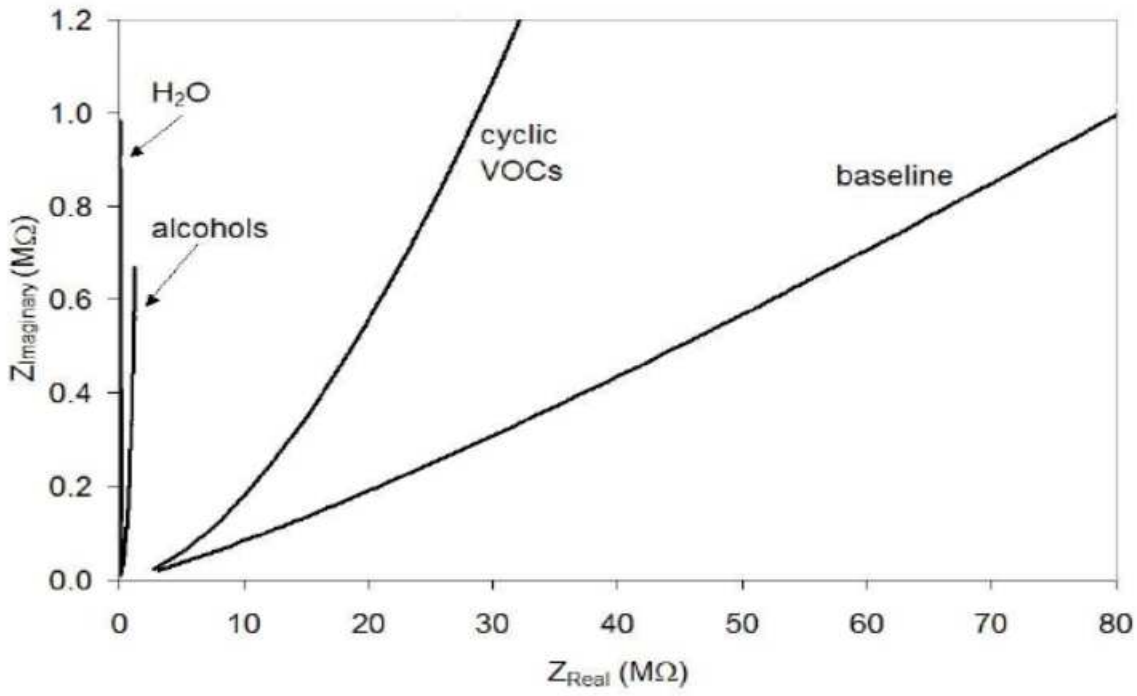

Figure 25 Cole-Cole plot of AAO sensor obtained in detecting various chemical analyte (Martin Kocanda et.al, 2009)

Table 2 Relative Permittivity Values of the Analytes

Name of the analyte	Relative permittivity
Water	78.50
Methanol	32.63
Isopropanol	16.30
n-heptane	1.93

Inspite of having least relative permittivity, n-heptane didn't show good response because of its hydrophobic nature and low polarity index, thus not forming covalent bonds with the NPO. Furthermore readings were taken during desorption of the analytes.

Figure 27 shows the desorption rate with various analytes in terms of its resistance. The rate of desorption of the analyte is directly dependent on their boiling points because if an analyte has higher boiling point then the rate of evaporation of that particular analyte will be lower. Table 3 shows the boiling point with respect to the analyte.

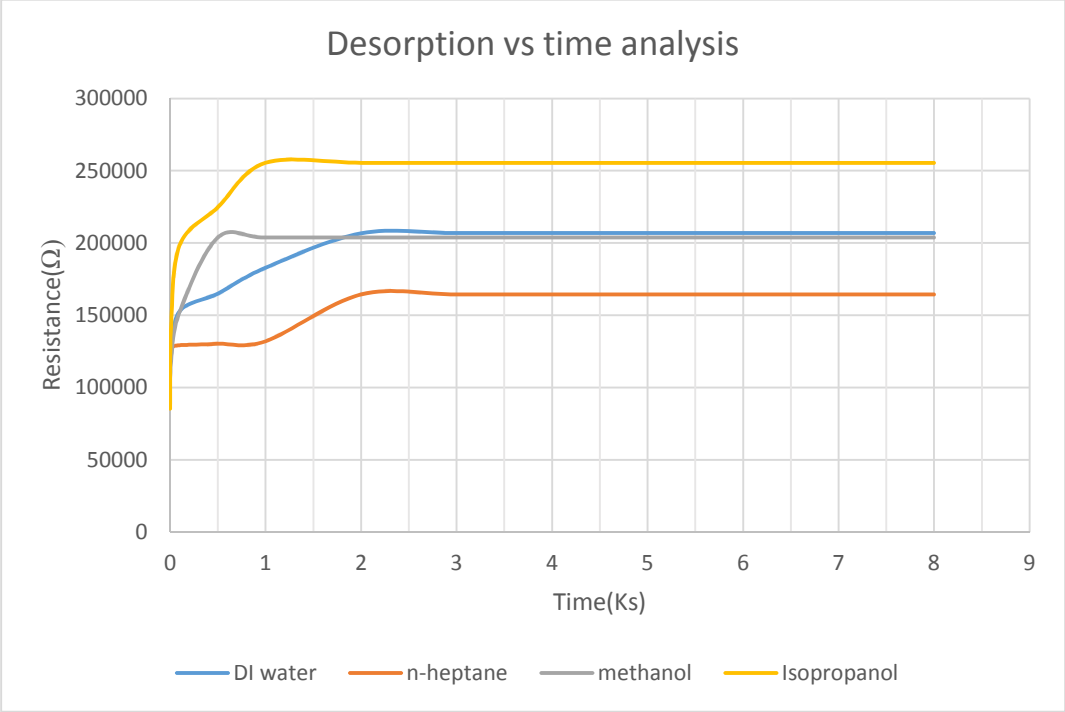

Figure 26 Analysis of the desorption rate of the plasma - treated NPO sensor in various analytes in time domain

Table 3 Boiling Points of the Analytes

Name of the analyte	Boiling point(ºC)

Water	100
Methanol	64.7
Isopropanol	86.20
n-heptane	98.42

As shown in Figure 27, the desorption of methanol occurs at ≈500s, isopropanol at ≈1 Ks, DI water at ≈2 Ks and n-heptane at ≈2 Ks. As both DI water and n-heptane have nearly same boiling points, their desorption is also at nearly 2 Ks. Thus it can be clearly stated that the desorption rates of the vapor analytes from the NPO surface is dependent on their respective boiling points.

3.4 Comparison of the NPO Sensor with AAO Sensor

The NPO sensor is now compared with the readings of the AAO sensor. The real and imaginary impedances of the AAO sensor are calculated using the same sensing setup used for that of the NPO. The resistance vs time and capacitance vs time graphs are obtained for the AAO sensor and are shown in Figure 28.

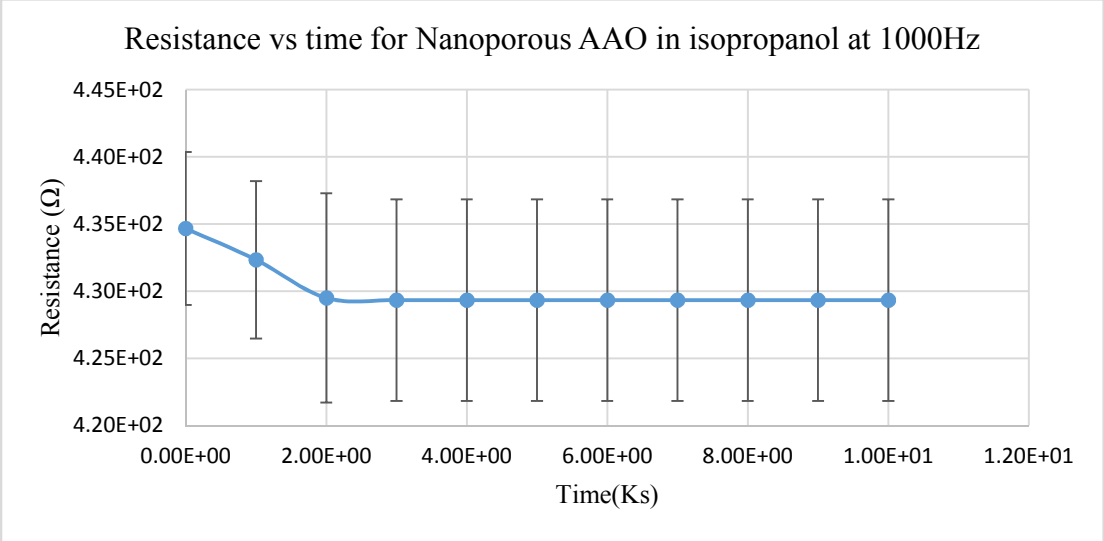

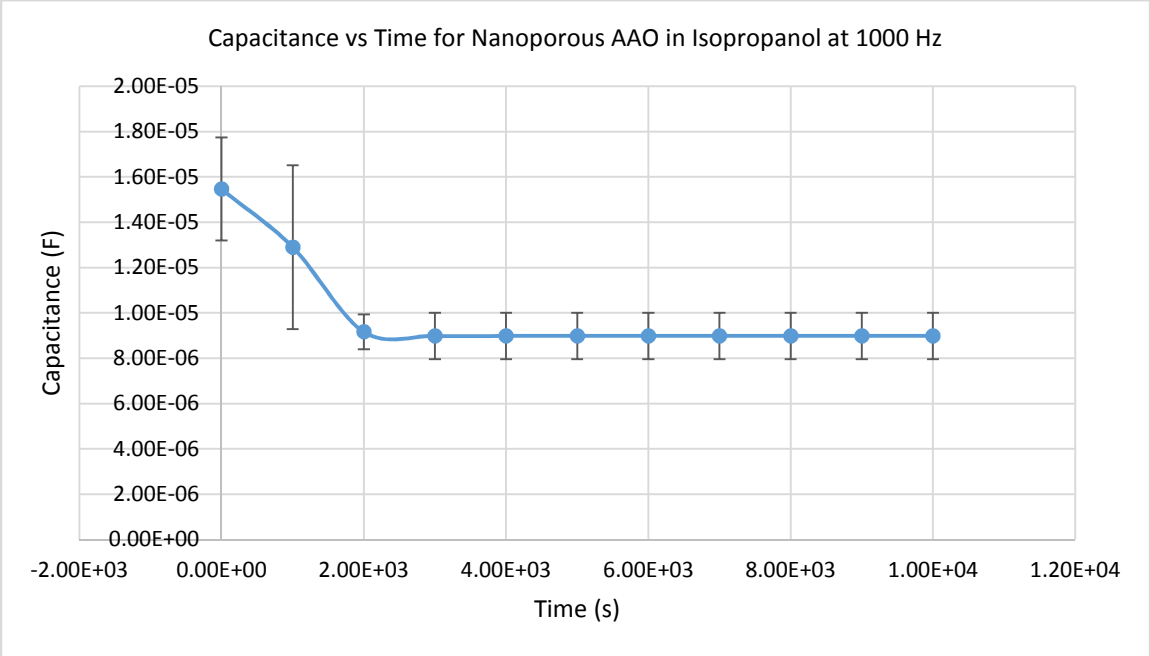

Figure 27 Time domain response of the nanoporous AAO sensor in isopropanol at 1000 Hz frequency

Figure 28 represents the resistance and capacitance in time domain of the nanoporous AAO in isopropanol at 1000 Hz frequency. When compared to that of the response of the NPO it could

be observed that the resistance of the NPO sensor is much higher compared to that of the nanoporous NPO sensor. This could be used to indicate that the NPO sensor has an ability to be a better performing sensor compared to that of the nanoporous AAO sensor.

Sensitivity of the sensor could also be calculated using the following formula:

$$\text{Sensitivity} = \frac{\text{Resistance of the sensor}}{\text{Resistance of the sensor at equilibrium in the analyte}} \times 100$$

From the above formula it could be calculated that sensitivity of the nanoporous AAO sensor in isopropanol is 101.1 % and the sensitivity of the NPO sensor in isopropanol is 300%. This proves that the NPO sensor is much more sensitive than that of the nanoporous AAO sensor with its sensitivity more than double the sensitivity of the AAO.

Chapter-4

CONCLUSION

In conclusion, we have reported on our preliminary experimentation of using nanoporous organosilicate thin films as sensor substrates. It showed that the nanoporous organosilicate films have distinguished between the various vapor - phase analytes used. However, the fabricated nanoporous organosilicate sensors (hydrophobic) exhibit sensitivity toward alcohol vapors with lower sensitivity to water vapor. But the plasma - treated nanoporous organosilicate sensor exhibit sensitivity toward alcohol vapors as well as water vapor with relatively low sensitivity toward n-heptane. The impedance spectrum (Nyquist plot) showed the hydrophilic sensor response in distinguishing of analytes depends on their relative permittivity, as in the case of nanoporous anodized aluminum oxide. It was also observed that the desorption rates of the vapor - phase analytes followed their respective boiling points. The impedance spectrum (Nyquist plot) observed depicted a typical parallel RC circuit, through which the equivalent circuit for the nanoporous organosilicate sensor could be represented as a parallel RC network.

The resistance values of the sensor recorded at different frequencies showed a very low resistance at higher frequencies, making the NPO sensor operated at lower frequencies rather than at higher frequencies. It was also observed the response of the adsorbed analytes followed their polarity: the analytes with higher polarity showed a larger change in their impedance values from the baseline.

Thus in conclusion, it could be demonstrated that the nanoporous organosilicate sensors can be used as a low-cost alternative to nanoporous anodized aluminum sensors as a chemical sensor. Future work can be done using more variety of analytes with cyclic volatile organic compounds and a mixture of compounds, analyzing if it could further discriminate from the mixture of analytes. Tunability can also be further examined, varying pore dimensions and porosity.

REFERENCES

[1] Anna C. Balazs, T. E. (2006). Nanoparticle Polymer Composites: Where Two Small Worlds Meet. *Sciece*, 1107-1110.

[2] Banica, F.-G. (2012). *Chemical Sensors and Biosensors: Fundamentals and Applications.* John Wiley & Sons.

[3] Chitra Agashe, R. C. (2008). High-yield synthesis of Nanocrystalline Tin dioxide by thermal decomposition for use in gas sensors. *The American ceramic society*.

[4] Christopher Radzik, G. K.-s. (2008). Electrical impedance response of a thick-thin film hybrid anodic nanoporous alumina sensor to methanol vapors. *International journal on smart sensing and intelligent systems*, 470-479.

[5] Dorf, R. C. (2006). *Sensors, Nanoscience, Biomedical Engineering, and Instruments.* Taylor and Francis group.

[6] F. Keller, M. S. (1953). Structural Features of Oxide Coatings on Aluminum. *Journal of the electrochemical society*, 411-419.

[7] G. Martin Kocanda, M. H.-S. (2009). Detection of cyclic volatile organic compounds using single-step anodized nanoporous alumina sensors. *IEEE sensors*, 1-6.

[8] GamryInstruments. (n.d.). Application-note. *Basics of Electrochemical Impedance spectroscopy*.

[9] Gösele, V. L. (1991). Porous silicon formation: A quantum wire effect. *Applied physics letters*, 856-858.

[10] IviumTechnologies. (n.d.). Product specification.

[11] J Hyeon-Lee, J. R. (2005). Properties of nanoporous organosilicate hybrid. *polymer international*, 772-779.

[12] Kiran Bhattacharyya, B. S. (2012). Gold nanoparticle mediated detection of circulating cancer cells. *Clinics in Laboratory Medicine*, 89-101.

[13] Licker, M. D. (2005). *Concise Encyclopedia of Science & Technology.* Mc Graw Hill.

[14] Losic, D. S. (2015). *Electrochemically Engineered Nanoporous Materials : Methods, Properties and Applications.* Springer.

[15] Mark E. Orazem, B. T. (2011). *Electrochemical Impedance Spectroscopy.* John Wiley & Sons.

[16] Morsi, Y. M. (2013). Ion Exchange Chromatography - An Overview. In D. F. Martin, *Column Chromatography* (pp. 1-30).

[17] NACL. (n.d.). *What's alumite?*

[18] Oomman K. Varghese, E. C. (2002). Room temperature ammonia and humidity sensing using highly ordered nanoporous Alumina films. pp. 91-110.

[19] The electric world. (1987). newyork: The W.J JoHnston Company.

[20] Venumadhav Korampally, M. Y. (2009). Entropy driven spontaneous formation of highly-porous films from polymer-nanoparticle composites. *Iopscience*, 1-7.

[21] W Lee, K. N. (2007). Self-ordering behavior of nanoporous anodic aluminum oxide (AAO) in malonic acid anodization. *Iopscience*.

[22] WOHLworks. (n.d.). Organic Analysis: Gas Chromatography.